URSI GASS 2020, Rome, Italy, 29 August - 5 September 2020

Notes on Radiofrequency and Plasma Coupling in Inductive Plasma Ion Sources

Marco Cavenago
INFN-LNL, viale dell'Universitá 2, 35020, Legnaro (PD) Italy, http://www.lnl.infn.it

Abstract

In the vast literature on waves and plasma interaction, the skin depth, the stochastic heating and the radiofrequency (rf) magnetic field effects emerge as important factors in simulations, still relying on effective collision rate models: a closed form and universal graph are given for stochastic heating. A simulation code based on iteration between plasma and rf calculations is recalled, and typical results are shown, for a simple induction ion source design.

1 Introduction

Radiofrequencies (rf) are often a convenient way to energize ion source plasma, from few MHz (inductive or capacitive coupling[1, 2, 3]) to GHz, as in electron cyclotron resonance (ECR) ion sources (ECRIS[4, 5]), see Fig 1. Heating may be enhanced by non-local effects as sheath and disuniformities; these anyway are often cast in local form, defining effective collision frequencies[6, 7, 8] in order to use efficient simulation tools[9, 10]. Let plasma be contained in a vessel (plasma chamber), say a cylinder of radius R_w and length L_p, and ω be the rf angular frequency and ω_p the plasma angular frequency

$$\omega_p = \sqrt{n_e e^2/(m_e \varepsilon_0)} \tag{1}$$

which depends on electron density n_e; conversely the cut-off density n_c is defined by $\omega = \omega_p$ that is $n_c = m_e \varepsilon_0 \omega^2/e^2$. Since we aim at $n_e \cong 10^{18}$ m^{-3} in an ion source, we have two major regimes: over 10 GHz we get $n_e < n_c$ (density below cut-off), waves propagates inside plasma, whose dimension L_p may easily exceed vacuum wavelength λ, as in ECRIS, typically used to produce multiply charged ions for nuclear physics experiments[4]. For MHz devices, we get $n_e > n_c$ (density over cut-off) so that rf electric field decays into plasma with typical distance δ (skin depth). In an inductively coupled device, see Fig. 1.(b), we have $\phi \cong 0$ (inside plasma) and $\mathbf{A} \cong \Re\, \hat{\vartheta} A_\vartheta(r,z) \mathrm{e}^{\mathrm{i}\omega t}$, where the operator $\Re$ (real part of) will be usually understood in the following (a phasor notation, widely used)[6, 8]; Maxwell's equations reduce to

$$r A_{\vartheta,zz} + (r A_{\vartheta,r})_{,r} + r Q A_\vartheta = \mu_0 \sigma U_k \tag{2}$$

with σ the conductivity, $2\pi U_k$ the voltage acting on the k-th turn of the coil, and $Q = -r^{-2} - \mathrm{i}\mu_0 \omega \sigma + \varepsilon_r (\omega/c)^2$ a combined function, where ε_r is the relative permittivity (excluding free currents featured by σ). Since the electron motion is very complicate[11, 12] inside plasma, see Fig. 2, the conductivity $\sigma = \check{\delta}\mathbf{j}/\check{\delta}\mathbf{E}$ is the functional derivative ($\check{\delta}$) of current $\mathbf{j}$ against the electric field $\mathbf{E}$, and σ is a tensor operator. But it is often convenient to approximate it by a scalar and local value $\sigma = n_e e^2/(\nu_c + \mathrm{i}\omega)$ with the collision frequency a sum $\nu_c = \nu_m + \nu_s$, where ν_m is due to particle collision and the so-called stochastic term ν_s is an averaged effect, extrapolated from more specific calculations, possible only in very simplified geometry and conditions. Then inside plasma or dielectrics

$$Q = \varepsilon_r \frac{\omega^2}{c^2} - \frac{1}{r^2} - \frac{\omega_p^2}{c^2} \frac{\mathrm{i}\omega}{\nu_c + \mathrm{i}\omega} \tag{3}$$

After this assumption, eq. (2) may be easily solved numerically (as for waves in lossy materials) to improve source design. In the similar ECR case[4, 5], expression for σ remains a tensor. Use of low ε_r dielectric windows is sometimes preferred to alumina ones ($\varepsilon_r = 9.8$).

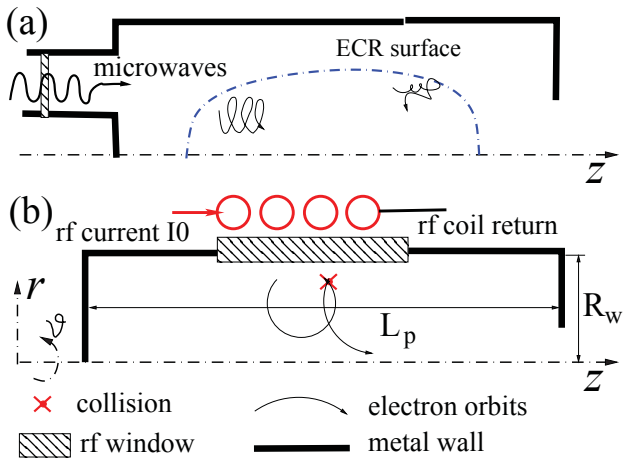

Figure 1. Schemes of typical rf ion sources: (a) ECRIS; (b) Inductively Coupled Plasma.

To calculate skin depth δ, we consider the planar geometry limit $y = r\sin\vartheta$ and $x = r\cos\vartheta - R_w$ with $R_w \to \infty$; for $x, y \ll R_w$ and $x < 0$ (plasma near wall) we have $A_\vartheta \cong A_y = a_1 \exp(\mathrm{i}k_x x)$ with phasor a_1, wavenumber $k_x = k_r - (\mathrm{i}/\delta)$ and k_r the real part of k_x. Let Q_∞ be the value of Q from eq. (3) without the term $1/r^2$, which is negligible in the planar

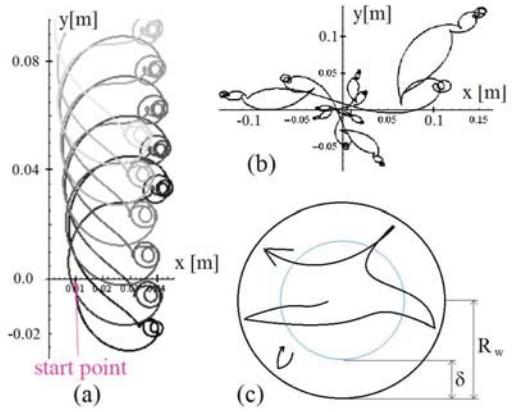

Figure 2. One electron motion in weak plasmas ($n_e \to 0$): (a) uniform rf field B_z and E_x; (b) uniform rf field B_z and $E_\vartheta \propto r$. For comparison scheme (c) includes rf shielding by strong plasma, note skin depth δ.

limit; thus $k_x = \sqrt{Q_\infty}$, and $\delta = -1/\Im k_x$. In detail

$$\delta = \frac{c\sqrt{2(1+\not{\nu}^2)}}{\sqrt{\omega_s^2 - \nu^2 + \sqrt{1+\not{\nu}^2}\sqrt{\omega_s^4 + \nu^2\omega^2}}} \tag{4}$$

with shorthands $\omega_s^2 = \omega_p^2 - \omega^2$ and $\not{\nu} = \nu_c/\omega$. As said before, typically $\omega_p \gg \omega, \nu$, so that also $\omega_s \gg \omega, \nu$; in the series expansion

$$\frac{\delta}{c} = \frac{\sqrt{2(1+\not{\nu}^2)}}{\sqrt{1+\sqrt{1+\not{\nu}^2}}}\frac{1}{\omega_s} + \frac{\sqrt{(1+\not{\nu}^2)/2}}{(1+\sqrt{1+\not{\nu}^2})^{3/2}}\frac{\omega^2}{\omega_s^3} + O\left(\frac{\omega^4}{\omega_s^5}\right) \tag{5}$$

it usually suffices to the first term only.

2 Models of Collisions

An electron approaching (or leaving) the wall with velocity v_x is subjected to rf for a time $\tau = \delta/|v_x|$; when τ is less than rf period $2\pi/\omega$, rf can efficiently heat electrons; according to Ref.[6], assuming thermal electrons with density n_e^w (at plasma limiting sheath near wall) and temperature T_e (in energy units), the adsorbed power P_w (per unit surface) is

$$\frac{P_w}{|E_w|^2} = n_e^w \frac{e^2\delta^2}{m_e v_{th}} I_1(\alpha) \quad , \quad \alpha = \frac{4\omega^2\delta^2}{\pi v_{th}^2} \tag{6}$$

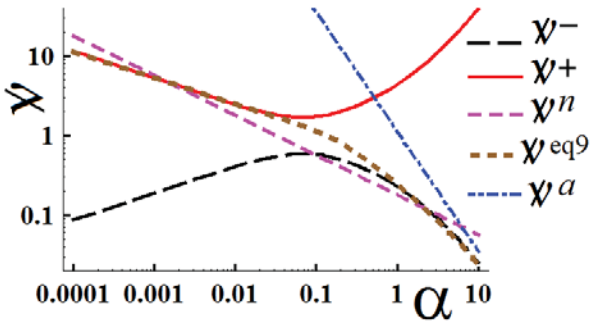

Figure 3. Plots of $\not{\nu}$ vs α, from eqs. (8) or (9).

$$I_1(\alpha) = [(1+\alpha)\mathrm{e}^\alpha \Gamma(0,\alpha) - 1]/\pi \tag{7}$$

where $E_w = \omega a_1/\mathrm{i}$ is electric field near dielectric wall, $v_{th} = (8T_e/\pi m_e)^{1/2}$ a thermal speed, and Γ the incomplete Gamma function. The adsorbed power for an effective collision rate ν_c is proportional to $\Re\, 1/(\nu_c + \mathrm{i}\omega)$; comparison gives

$$\frac{\not{\nu}}{1+\not{\nu}^2} \cong 2\sqrt{\pi\alpha} I_1(\alpha) \equiv I_2(\alpha) \tag{8}$$

with $\not{\nu} = \nu_c/\omega$; the two solution branches $\not{\nu}^\pm(\alpha)$ are shown in Fig. 3. In the limit $\alpha \to \infty$ (that is $\tau \gg 2\pi/\omega$ for most electrons) no efficient heating of electrons can expected, so the lower branch should be selected; but its leading term[6] $\not{\nu}^a = 2/\sqrt{\pi\alpha^3}$ is not accurate for $\alpha < 10$. For the case $\alpha \ll 0.01$ we expect large rf effects for most electrons, so the upper branch $\not{\nu}^+$ should be used; a naive estimate is about $\not{\nu}^n = 1/\sqrt{\pi^3\alpha}$, which fails over $\alpha > 0.01$. Much more accurate expression are obtained by fits of $\not{\nu}^-$ for large α and of $\not{\nu}^+$ for small α values[9]; an elaborate fit including and joining both cases is known[7]. Moreover, by considering the singularity of the Γ function for $\alpha \to 0$ and joining term to the expansion for large α, we propose:

$$\not{\nu} = \frac{\sqrt{1/\pi}}{\sqrt{2\alpha^2 + \frac{1}{4}\alpha^3 + \alpha\left[2 + \frac{4}{\pi^2}\log^2(c_1/\alpha)^2\right]}} \tag{9}$$

with $c_1 = \mathrm{e}^{-1-\gamma} \cong 0.206$ and $\gamma \cong 0.577$ the Euler's constant; eq. (9), as shown in Fig. 3, matches correctly the limiting cases of $\not{\nu}^\pm$ and interpolates them smoothly for intermediate values of α. These values must be included in simulations (since δ and α can take any positive value) and it is the region of more effective heating; so results may be sensitive to $\not{\nu}(\alpha)$ interpolation. Another relation between $\not{\nu}$ and α comes from δ expressions (computed before); inserting v_{th} and eq. (5) into eq. (6) (and keeping only the leading term in ω_p/ω) gives

$$\alpha = \frac{m_e\omega^2\delta^2}{2T_e} \cong \frac{1}{X}\frac{1+\not{\nu}^2}{1+\sqrt{1+\not{\nu}^2}} \tag{10}$$

$$X \equiv \frac{T_e\omega_s^2}{m_e c^2\omega^2} \cong \frac{n_e^w T_e}{p_0} + O\left(\frac{\omega^2}{\omega_p^2}\right) \quad , \quad p_0 = \frac{m_e^2\omega^2}{\mu_0 e^2} \tag{11}$$

with X the ratio between plasma electron pressure and a reference p_0 which depends only from ω; in our case, $\omega = 1.269 \times 10^7$ rad/s and $p_0 = 4.144 \times 10^{-3}$ Pa. Numerical solution of Eqs. (9) and (10) for any given X is easily calculated; the lower bound $\alpha_0 = (c_0/X)^{3/4}$ with $c_0 = 0.394$ is used as starting point; results are shown in Fig. 4. In summary, stochastic collision rate is a function of electron plasma pressure against wall sheath, which phenomenological view well deserves to be tested with future kinetic calculations. In general an effective collision rate may be defined $\nu_e = \Re\, n_e e^2/(m_e\sigma)$.

3 Magnetic Field: Static and rf Terms

The effect of rf magnetic field B_f can be simply discussed in cylindrical geometry, only for $\omega r \ll c$ and at plasma onset

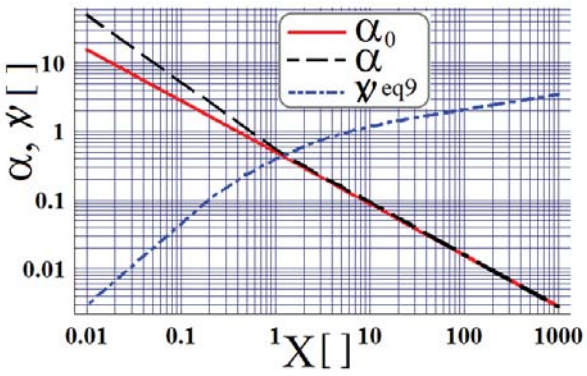

Figure 4. Plot of ψ and α vs parameter $X = n_e^w T_e/p_0$.

$n_e \cong 0$ and without z dependencies. Then $Q \cong -1/r^2$ and eq. (2) admits the solution $A_\vartheta = a_2 r$ inside plasma with $a_2 = \mathrm{i}B_f/2$. Adding a static magnetic field $B_s\hat{z}$ to our ion source we have $B_z = B_f \sin\psi + B_s$ and $E_\vartheta = \frac{1}{2}\omega r B_f \cos\psi$ with the shorthand $\psi = \omega t$; let $\Omega_s = eB_s/m_e$ be the usual cyclotron angular frequency due to static field and $\Omega_f = eB_f/m_e$ the one due to rf field. The electron motion equation

$$m_e\dot{\mathbf{v}} = -e(\mathbf{E} + \mathbf{v}\times\mathbf{B}) - m_e\nu_m\mathbf{v} \qquad (12)$$

becomes, with the coordinate $x_c = x + \mathrm{i}y$ (so that $r = |x_c|$):

$$\ddot{x}_c + M\dot{x}_c + \mathrm{i}\omega k_1 x_c \cos\psi = 0 \quad , \qquad (13)$$

where $M = k_0 + 2ik_1\sin\psi$ with values $k_0 = \nu_m + \mathrm{i}\Omega_s$ and $k_1 = \frac{1}{2}\Omega_f$. When $k_1 = 0$ (no rf) we get the usual damped cyclotron oscillation $x_c = x_0 \mathrm{e}^{i\Omega t}$ with angular frequency $\Omega = \mathrm{i}k_0$, whose real part is $-\Omega_s$; otherwise parametric resonances may occur (Hill or Mathieu equation), including $\Omega = -\mathrm{i}s + n\omega$ terms with n any integer and s the complex growth rate. Averaging the current I_ϑ per electron on all orbits passing through a given x_c point and taking only 1st harmonic gives a typical result as[12]:

$$\langle I_\vartheta/E_\vartheta\rangle \cong (e^2/m)[f(-\omega,k_0,k_1) + f^*(\omega,k_0,k_1)], \qquad (14)$$

$$f(\omega,a,b) \cong \frac{5/2}{2a - i\omega + 3\sqrt{(a+2i\omega)^2 + (15/4)b^2}} \qquad (15)$$

Then $\langle\sigma\rangle \cong n_e\langle I_\vartheta/E_\vartheta\rangle$ for constant ν_m. When B_f is small (linear rf) we have resonances at $\omega = \pm\Omega_s$, as in ECR.

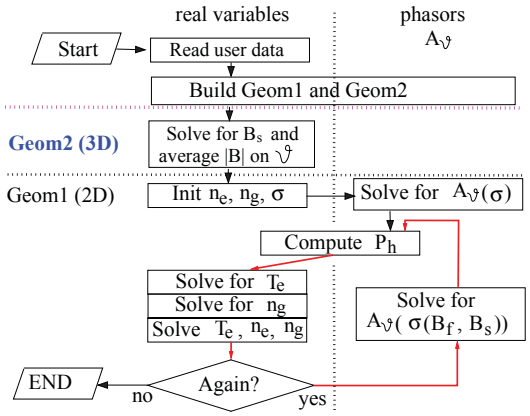

Figure 5. Major steps of numerical simulations.

In the case $B_s = 0$ and $\Omega_t = \Omega_f$ an effective conductivity approximation, more convenient for following simulations and valid also for large n_e, was proposed[8]:

$$\sigma = \frac{n_e e^2}{m_e\sqrt{\nu_m^2 + \Omega_t^2}}\left(1 - \frac{i\omega\nu_m}{\nu_m^2 + \Omega_t^2} + O(\nu_m^2)\right) \qquad (16)$$

assuming $\omega \ll \nu_m < \Omega_t$; for $B_s \neq 0$ we generalize it taking $\Omega_t^2 = \frac{1}{2}\Omega_f^2 + \Omega_s^2$. The latter estimate roughly expresses reduction of conductivity and electron mobility due to $|B|$.

4 Simulations and Results

For noble gases, the flow $\mathbf{\Gamma}_e$ of electrons and the flow $\mathbf{\Gamma}_i$ of ions are related by quasineutrality inside plasma:

$$\mathrm{div}\,\mathbf{\Gamma}_i = \mathrm{div}\,\mathbf{\Gamma}_e = n_g n_e K_{iz}(T_e) = n_{iz} \qquad (17)$$

where $K_{iz}(T_e)$ is the ionization coefficient[2], n_g is the gas density and n_{iz} the ionization rate (per unit volume and time); for other gases, negative and molecular ions can be included, possibly with some effective K_{iz}. The gas density n_g may in principle be related to input gas density n_0 by $C_0(n_0 - n_g) - C_1 n_g \cong \int \mathrm{d}^3x\, n_{iz}/i_z$ where C_0 is the conductance of gas input to source, C_1 the one of gas exit and $i_z \cong 1$; or be adjusted by the code to improve rf coupling. A simplified thermal energy balance[8, 12] is written as:

$$-\nabla(K_e\nabla T_e) = P_h - n_e n_g K_{iz}\mathscr{E}_{iz} \quad , \quad P_h = \tfrac{1}{2}\Re(j_\vartheta^* E_\vartheta) \qquad (18)$$

where K_e is thermal conductivity and $\mathscr{E}_{iz}$ total energy lost per ionization[2]. Ion flow due to ambipolar potential is

$$\mathbf{\Gamma}_i = -D_a(\mathbf{B}_s)\nabla\left(n_e + \frac{B_f^2}{4\mu_0 T_e}\right) \qquad (19)$$

with the ambipolar diffusion tensor D_a, and the B_f^2 term partly balancing the n_e gradient. Plasma simulations with eq. (8) assumption (or equivalently Fig. 4 data) for ψ where described in Ref. [7]. As for the model of eqs. (2,16-19), an iterative solution is necessary to calculate A_ϑ (complex) updating P_h, T_e and then n_g, n_e at each step, see Figs. 5 and 6; this staging also aims to keep n_e and T_e real valued, protecting them from rounding errors and numerical instability. Due to 20% typical accuracy of K_{iz} data and difficulties of numerical convergence, some careful initialization is

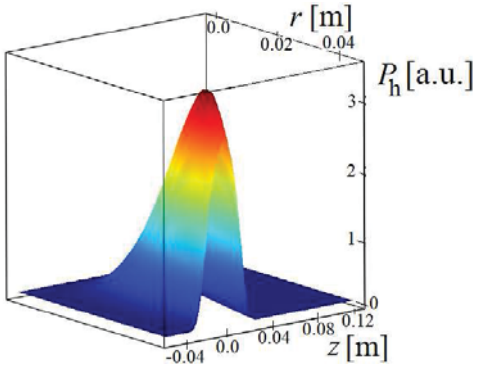

Figure 6. Plasma heating power density P_h.

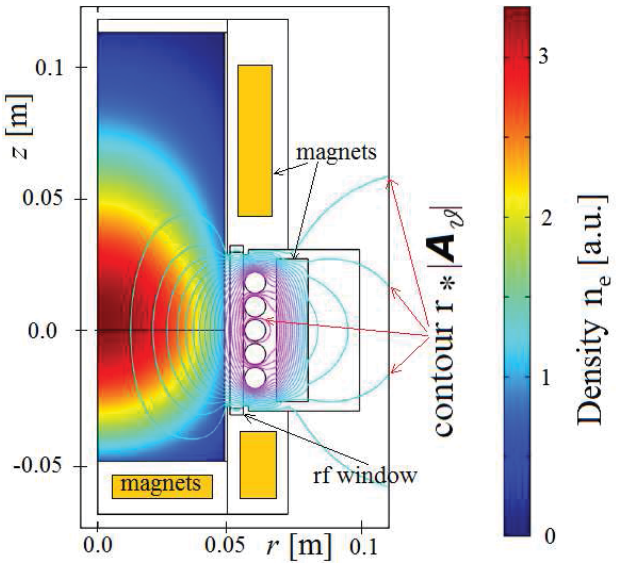

Figure 7. Plasma density n_e and 'pseudo-flux-lines' of rf magnetic field (that is, level curve of $r|A_\vartheta|$).

necessary to keep result precision in that range. Samples of results with a preliminary NIO1[7] geometry (5 turn rf coil instead of 7 turns) are shown in Figs. 6 and 7. In this model the voltages U_k are adjusted so that the currents I_k integrated on the k-th coil turn section match an assigned input rf current I_0; then total coil voltage is $V = 2\pi\sum_k U_k$ and equivalent coil resistance is simply $R_t = \Re V/I_0$; as a check power dissipated P_h^i in all model regions i is calculated (with $i = (p)$ referring to plasma) defining resistances $R_i = 2P_h^i/|I_0|^2$, and relation $R_t \cong \sum_i R_i$ is verified (typically within 1 %).

In conclusion, heating efficiency $\eta = R^{(p)}/R_t$ can exceed 0.5 with adequate central densities n_{e0} and gas pressures p_g (see Fig. 8 with $n_0^r \cong 10^{17}$ m^{-3}), which is a starting point for a robust design. Moreover, thanks to a static multipole field $B_s \cong 5$ mT near wall and to B_f term in eq. (19), heating maximum occurs before wall (at $r \leq 0.04$ m$< R_w$ in our example of Fig. 6) protecting window at $R_w = 0.05$ m, but reducing somewhat efficiency. This may stabilize plasma discharge when current I_0 exceed the threshold for producing larger n_e densities and help rf matching.

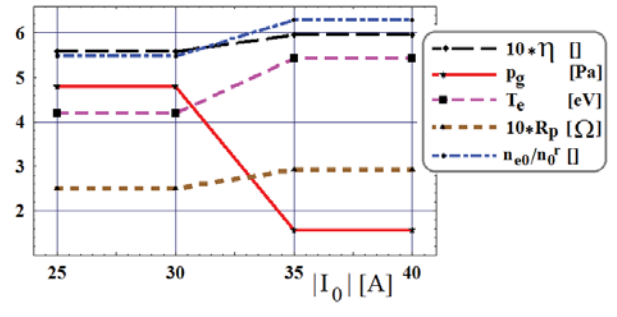

Figure 8. Preliminary simulation results (see legend for units and text for definition and errors) vs rf current $|I_0|$.

References

[1] M. A. Lieberman and V. A. Godyak, "From Fermi Acceleration to Collisionless Discharge Heating," *IEEE Trans. Pla. Sci.*, **26**, 1998, pp. 955–986, doi:10.1109/27.700878.

[2] M. A. Lieberman and A. J. Lichtenberg, "Principles of Plasma Discharges and Materials Processing," New York, Wiley, 2005 (2nd ed.), doi:10.1002/0471724254.

[3] I. D. Kaganovich, V. I. Kolobov, and L. D. Tsendin, "Stochastic electron heating in bounded radio-frequency plasmas" *Appl. Phys. Lett.*, **69**, 1996, pp. 3818–3820, doi:10.1063/1.117115.

[4] G. Torrisi, D. Mascali, A. Galatà, et al., "Plasma heating and innovative microwave launching in ECRIS: models and experiments," *J Instrum*, **14**, 2019, C01004, and references therewithin, doi:10.1088/1748-0221/14/01/C01004.

[5] M. Cavenago and C. T. Iatrou, "Studies on microwave coupling into the electron cyclotron resonance ion source Alice," *Rev. Sci. Instrum.*, **65**, 1994, pp 1122–1124, doi:10.1063/1.1145084.

[6] V. Vahedi, M. A. Lieberman, G. DiPeso, T. D. Rognlien, and D. Hewett, "Analytic model of power deposition in inductively coupled plasma sources," *J. Appl. Phys.*, **78**, 1995, pp. 1446–1458, doi:10.1063/1.360723.

[7] M. Cazzador, M. Cavenago, G. Serianni, and P. Veltri, "Semi-analytical modeling of the NIO1 source," *AIP Conf. Proc.*, **1655**, 2015, 020014, doi:10.1063/1.4916423.

[8] M. Tuszewski, "Inductive electron heating revisited," *Phys. Plasmas*, **4**, 1997, pp. 1922–1928, doi:10.1063/1.872335.

[9] P. Jain, M. Recchia, M. Cavenago, U. Fantz, E. Gaio, W. Kraus, A. Maistrello and P. Veltri, "Evaluation of power transfer efficiency for a high power inductively coupled radiofrequency hydrogen ion source," *Plasma Phys. Control. Fusion*, **60**, 2018, 045007, doi:10.1088/1361-6587/aaab19.

[10] D. Rauner, S. Briefi and U. Fantz, "RF power transfer efficiency of inductively coupled low pressure H2 and D2 discharges," *Plasma Sources Sci. Technol.*, **26**, 2017, 095004, doi:10.1088/1361-6595/aa8685.

[11] F. F. Chen, "Nonlinear Effects and Anomalous Transport in RF Plasmas," *IEEE Trans. Pla. Sci.*, **34**, 2006, pp. 718–727, doi:10.1109/TPS.2006.874851.

[12] M. Cavenago and S. Petrenko, "Models of radiofrequency coupling for negative ion sources," *Rev. Sci. Instrum.*, **83**, 2012, 02B503, doi:10.1063/1.3670601.